

Article

Controlled Hydrothermal Precipitation of Alunite and Natroalunite in High-Aluminum Vanadium-Bearing Aqueous System

Luyao Wang^{1,2,3} , Nannan Xue^{1,2,3,*}, Yimin Zhang^{1,2,3,4,*} and Pengcheng Hu^{1,2,3}

¹ School of Resource and Environmental Engineering, Wuhan University of Science and Technology, Wuhan 430081, China; 15671552595@163.com (L.W.); hpcmy126@126.com (P.H.)

² State Environment Protection Key Laboratory of Mineral Metallurgical Resources Utilization and Pollution Control, Wuhan University of Science and Technology, Wuhan 430081, China

³ Collaborative Innovation Center of Strategic Vanadium Resources Utilization, Wuhan 430081, China

⁴ Hubei Provincial Engineering Technology Research Center of High Efficient Cleaning Utilization for Cleaning Utilization for Shale Vanadium Resource, Wuhan University of Science and Technology, Wuhan 430081, China

* Correspondence: cbd@aliyun.com (N.X.); zym126135@126.com (Y.Z.); Tel./Fax: +86-027-6886-2057 (Y.Z.)

Abstract: During the acid leaching process of black shale, with the destruction of the aluminosilicate mineral structure, a large amount of aluminum (Al) is leached, accompanied by the release of vanadium (V). To separate aluminum from the vanadium-containing solution, the precipitation behavior of aluminum ions (Al^{3+}) was investigated under hydrothermal conditions with the formation of alunite and natroalunite. In the solution environment, alunite and natroalunite are able to form stably by the Al^{3+} hydrolysis precipitation process at a temperature of 200 °C, a pH value of 0.4 and a reaction time of 5 h. When Al^{3+} was precipitated at a K/Al molar ratio of 1, the aluminum precipitation efficiency and the vanadium precipitation efficiency were 64.77% and 1.72%, respectively. However, when Al^{3+} was precipitated at a Na/Al molar ratio of 1, the precipitation efficiency of the aluminum decreased to 48.71% and the vanadium precipitation efficiency increased to 4.36%. The thermodynamics and kinetics results showed that alunite forms more easily than natroalunite, and the reaction rate increases with increasing temperature, and the precipitation is controlled by the chemical reaction. Vanadium loss increases as the pH value increases. It can be deduced that the ion state of tetravalent vanadium (VO_2^{2+}) was transformed into the ion state of pentavalent vanadium (VO_2^+) in the hydrothermal environment. The VO_2^+ can be adsorbed on the alunite or natroalunite as a result of their negative surface charges, ultimately leading to vanadium loss.

Keywords: aluminum; black shale; alunite; natroalunite; hydrothermal precipitation



Citation: Wang, L.; Xue, N.; Zhang, Y.; Hu, P. Controlled Hydrothermal Precipitation of Alunite and Natroalunite in High-Aluminum Vanadium-Bearing Aqueous System. *Minerals* **2021**, *11*, 892. <https://doi.org/10.3390/min11080892>

Academic Editors:
Przemyslaw B. Kowalczyk

Received: 28 June 2021

Accepted: 12 August 2021

Published: 18 August 2021

Publisher's Note: MDPI stays neutral with regard to jurisdictional claims in published maps and institutional affiliations.



Copyright: © 2021 by the authors. Licensee MDPI, Basel, Switzerland. This article is an open access article distributed under the terms and conditions of the Creative Commons Attribution (CC BY) license (<https://creativecommons.org/licenses/by/4.0/>).

1. Introduction

Black shale is an important and abundant vanadium-bearing resource in China, and has attracted much attention from researchers [1–3]. In vanadium-bearing black shale, vanadium (V) mainly exists as low-valence V(III) in the crystal lattice of the muscovite, replacing aluminum (Al) due to their isomorphism [4,5]. The main distribution of vanadium grade in black shale deposits is in the range 0.1–1.0%; only 2.8% of black shale possesses a vanadium grade over 1.0%. Thus, the mica structure needs to be destroyed in order to release vanadium from the black shale. In the alkaline leaching process, the silica present in black shale can react with alkali to form colloidal silica, which makes it difficult to separate vanadium-bearing alkali leachate from residue. Acid leaching is usually adopted for the extraction of vanadium from black shale [6,7]. The aluminum is leached along with the vanadium, inevitably increasing the aluminum concentration to 15–20 g/L, which is far higher than the vanadium concentration. The separation of vanadium over aluminum has become the core scientific problem in the purification and concentration of high-aluminum vanadium-bearing leachate.

In high-aluminum vanadium-bearing leachate, the aluminum ions spontaneously transform into colloidal alum ($\text{KAl}(\text{SO}_4)_2 \cdot 12\text{H}_2\text{O}$), which can adsorb vanadium ions, causing vanadium loss [8]. Meanwhile, aluminum ions have adverse effects on the subsequent processes of solvent extraction or the precipitation process of vanadium by acidic ammonium salt. It has been reported that aluminum ions can be co-extracted with vanadium ions, which reduces the extraction efficiency of vanadium in D2EHPA(P204) solvent extraction systems [9,10]. Moreover, aluminum ions can also be adsorbed onto vanadium precipitates (such as poly-ammonium vanadate) or be precipitated in the form of alum in the vanadium precipitation process by acidic ammonium salt, leading to low crystallinity of poly-ammonium vanadate, and ultimately reducing the purity of the vanadium pentoxide [8,11].

It has been noticed by some scholars [12] that in the pH range of 3–5, aluminum hydroxide forms. Wang [12] adopted 8-hydroxyquinoline as the selective complexing precipitant at a pH value of 4.5, leading to the precipitation of aluminum ions in the form of 8-hydroxyquinoline aluminum. However, the vanadium is easy to hydrolyze and precipitate in the pH range of 2–4 [13,14]. Therefore, the above-mentioned methods with aluminum hydroxide or 8-hydroxyquinoline aluminum precipitation are suitable for achieving no vanadium co-existence. Guo [15] found that the cooling crystallization of $\text{AlCl}_3 \cdot 6\text{H}_2\text{O}$ from the high-aluminum acid leaching solution of coal gangue was an effective method for the removal of aluminum. However, the high consumption of hydrochloric acid dilutes the concentrations of valuable ions, resulting in an increase in the number of extraction stages. Shi [11] also adopted the method of cooling crystallization to remove aluminum in the form of $\text{KAl}(\text{SO}_4)_2 \cdot 12\text{H}_2\text{O}$ from the high-aluminum vanadium-bearing leachate of black shale. After a long period of crystallization, the aluminum precipitation efficiency reached no more than 70%. Apparently, it is necessary to find an efficient and feasible method for the removal of aluminum from high-aluminum vanadium-bearing leachate.

Alunite ($\text{KAl}_3(\text{SO}_4)_2(\text{OH})_6$) and natroalunite ($\text{NaAl}_3(\text{SO}_4)_2(\text{OH})_6$) belong to the alunite supergroup ($\text{AB}_3(\text{TO}_4)_2(\text{OH})_6$) and form stably in oxidizing, acidic, and $\text{SO}_4^{2-}/\text{Al}^{3+}$ -enriched hydrothermal environments [16,17], especially at hydrothermal temperatures of above 100 °C. The increasing temperature obviously offsets the initial reaction acidity for Al^{3+} hydrolysis and promotes the formation of alunite and natroalunite [18]. The K/Al molar ratio also changes the stoichiometric number of alunite [19]. Some scholars have successfully synthesized natroalunite at acidic pH values (1–4) and temperatures no less than 180 °C in order to immobilize As, or adsorb F^- , Cd^{2+} , PO_4^{3-} from the aqueous solution [20–22]. It has been reported that alunite can be formed in the pressure acid leaching process of black shale, and the hydrolyzation of Al could be initiated more easily than that of vanadium by reducing the residual acid of the leachate [23,24]. Therefore, both alunite and natroalunite can be considered new aluminum-containing precipitates for the separation of vanadium over aluminum on the basis of their resistance to acidic and high-temperature conditions. However, the generation difference between alunite and natroalunite has not been clarified in the existing published literature, which is important for the theoretical guidance of the purification process of high-aluminum vanadium-bearing acid leaching solutions of black shale.

In this paper, to effectively separate aluminum and vanadium, the effect of the main parameters on the precipitate efficiency of aluminum was studied, namely pH values, K(or Na)/Al molar ratios and temperatures. Meanwhile, the precipitation behaviors of alunite and natroalunite were compared on the basis of analysis of their thermodynamics and kinetics. Finally, the phase composition, elemental distribution, and surface charge of the precipitate were analyzed to clarify the mechanism of vanadium and alunite co-precipitation.

2. Experimental Section

2.1. The Removal Behavior of Al in Acid Solution

The main metal impurity ions in the acid leachate of black shale are Al^{3+} , Fe^{3+} , Fe^{2+} , Mg^{2+} , K^+ , Na^+ and Ca^{2+} . In the alunite supergroup ($\text{AB}_3(\text{TO}_4)_2(\text{OH})_6$), the A site is usually occupied by a monovalent cation (such as K^+ , Na^+) or a divalent cation (such as Ca^{2+} , Ba^{2+} , Pb^{2+}), the B site is principally occupied by Al^{3+} and Fe^{3+} [20]. During the formation of alunite or natroalunite, the Fe^{3+} and Ca^{2+} can be embedded in the crystal lattice of alunite. To avoid the influence of Fe^{3+} , Ca^{2+} and the formation of K-Na alunite on the aluminum precipitation process, the vanadium-bearing solution was obtained by dissolving VO_2SO_4 and $\text{Al}_2(\text{SO}_4)_3 \cdot 18\text{H}_2\text{O}$ in deionized water. The K_2SO_4 or Na_2SO_4 was fed into the vanadium-bearing solution to a certain volume with a certain K(or Na)/Al molar ratio, and mixed adequately. The concentration of vanadium and aluminum in the solution were 1.79 g/L and 0.6 mol/L, respectively.

Then, the mixed solution was put into the pressurized reactor (MCT250, Beijing Century SenLong experimental apparatus Co., Ltd., Beijing, China), and kept at a certain temperature for a specified time. After the reaction, the solution and precipitate were separated by filtration. All reagents used in the tests were analytically pure. Deionized water was used throughout. The precipitation efficiency (η) of aluminum and vanadium were calculated using the following equation (see Equation (1)):

$$\eta = \frac{C_0 \times V_0}{C \times V} \times 100\% \quad (1)$$

where η is the precipitation efficiency of aluminum or vanadium (%), C_0 is initial concentration of aluminum or vanadium in solution before reaction (g/L), V_0 is the solution volume before reaction (L), C is the concentration of aluminum or vanadium ions in solution after reaction (g/L), V is the solution volume after reaction (L).

The kinetic experiment was carried out in a pressurized reactor. An amount of 200 mL solution was added into the reactor, and the initial pH value of the solution was 0.6. During the 4 h reaction, 2 mL of the solution was taken out from the sampling tube of the reactor at intervals, and the concentration of K^+ or Na^+ was measured by the Ion chromatograph.

2.2. Detection Methods

The concentration of vanadium in the solution was analyzed by titration with ferrous ammonium sulfate. The phase compositions of the samples were tested by means of X-ray diffraction (XRD, D/MAX 2500PC, Rigaku, Tokyo, Japan) using $\text{Cu K}\alpha$ radiation. Microscopic observation and elemental analysis were conducted with a scanning electron microscope (SEM, JSM-IT300, JEOL, Tokyo, Japan) equipped with an energy dispersive spectrometer (EDS, X-Act, Oxford, London, UK). The pH value of the solution was measured using a pH meter (PHS-3C, INESA Scientific Instrument Co., Ltd. Shanghai, China). The aluminum concentration of the solution was obtained using ICP-AES (Optima-4300DV, PerkinElmer, Boston, MA, USA). The Na^+ or K^+ concentration in solution was obtained by Ion chromatography (Metrohm 883, Heriau, Switzerland). X-ray photoelectron spectroscopy (XPS) analysis was conducted using a Multilab 2000 instrument (ThermoFisher Electron, Waltham, MA, USA). The zeta potential was measured using a Zetasizer nano potentiometric titrator (Malvenpanako, Almelo, The Netherlands).

3. Results and Discussion

3.1. Effect of Initial pH Value on the Precipitation Efficiency of Al

To determine whether the addition of sodium sulfate or potassium sulfate can effectively remove aluminum from the vanadium-bearing solution under different pH values, experiments were conducted at different pH values under the following conditions: a temperature of 200 °C, K(or Na)/Al molar ratio of 1, and reaction time of 5 h. The pH values after the reaction are shown in Table 1, and the precipitation efficiency of aluminum

and vanadium are shown in Figure 1. The phase composition of the precipitates obtained at a pH value of 0.6 were analyzed by XRD, and the results are shown in Figure 2.

Table 1. The pH value of the solution before and after reaction.

pH Value	Na ₂ SO ₄					K ₂ SO ₄				
	0	0.3	0.4	0.6	0.8	0	0.3	0.4	0.6	0.8
Before reaction	0	0.3	0.4	0.6	0.8	0	0.3	0.4	0.6	0.8
After reaction	0	0.29	0.21	0.41	0.39	−0.10	0.27	0.25	0.51	0.54

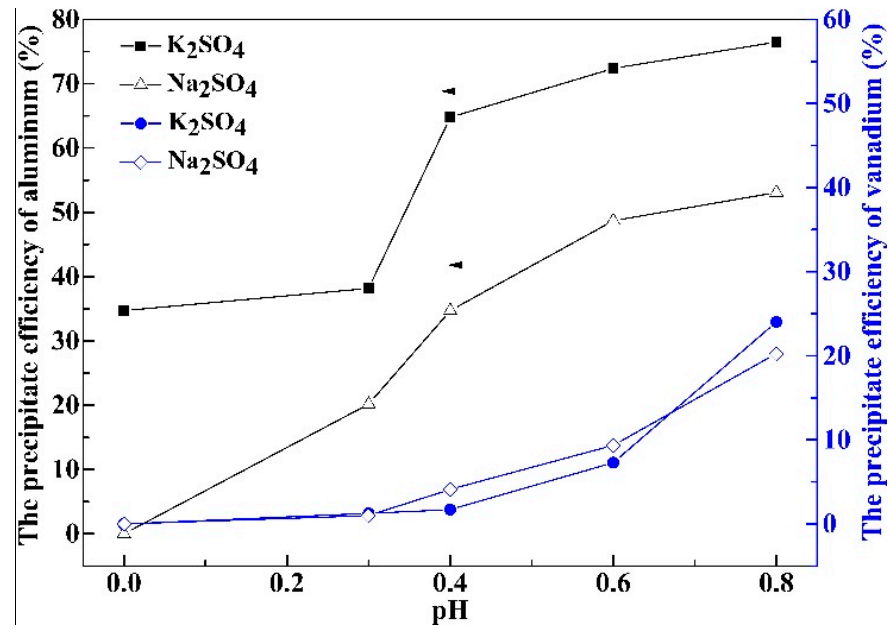


Figure 1. Effect of pH value on the precipitation efficiency of aluminum and vanadium.

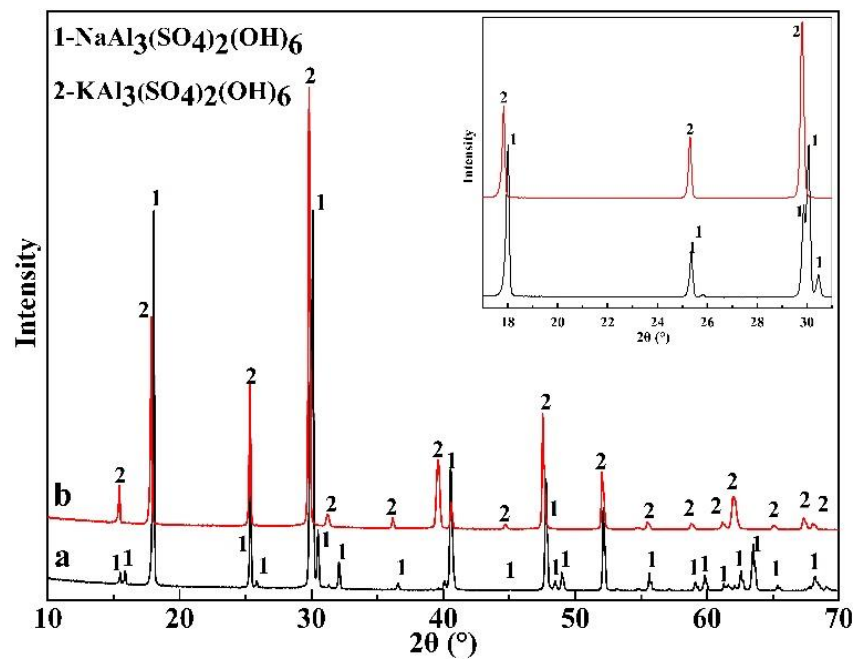


Figure 2. XRD patterns of precipitate obtained at pH value of 0.4: (a) Na₂SO₄; (b) K₂SO₄.

As shown in Table 1, the pH value decreased after the reaction, indicating that H^+ was produced in the reaction process.

It can be seen from Figure 1 that the pH value significantly influenced the precipitation behavior of aluminum. With increasing pH value, the precipitation efficiency of aluminum also increased. However, at the same pH value, the precipitation efficiency of aluminum with the addition of sodium sulfate was lower than that with the addition of potassium sulfate. When the pH value was 0.4, the precipitation efficiency of aluminum with the addition of potassium sulfate was 64.77%, while the precipitation efficiency of aluminum with the addition of sodium sulfate was only 48.71%. However, the precipitation efficiency of vanadium was 1.72% and 4.36%, respectively. When the pH value exceeded 0.6, the precipitation efficiency of vanadium increased rapidly, indicating an increase in the loss of vanadium. Thus, under the same conditions, potassium sulfate is more suitable for the removal of aluminum than sodium sulfate. To avoid vanadium loss, the initial pH value of solution should not be more than 0.4.

When the initial pH value is less than 0.8, the precipitate is white. Figure 2 clearly shows that only the natroalunite ($NaAl_3(SO_4)_2(OH)_6$) or alunite ($KAl_3(SO_4)_2(OH)_6$) is detected, without the appearance of any other diffraction peaks. Hence, it is feasible to remove aluminum from the vanadium-bearing acid solution with the formation of alunite and natroalunite.

3.2. Effect of K(Na)/Al Molar Ratio on the Precipitation Efficiency of Al

Experiments were performed using different K(or Na)/Al molar ratios under the following conditions: pH value of 0.4, temperature of 200 °C, and reaction time of 5 h. The results obtained after the reaction were as shown in Figure 3.

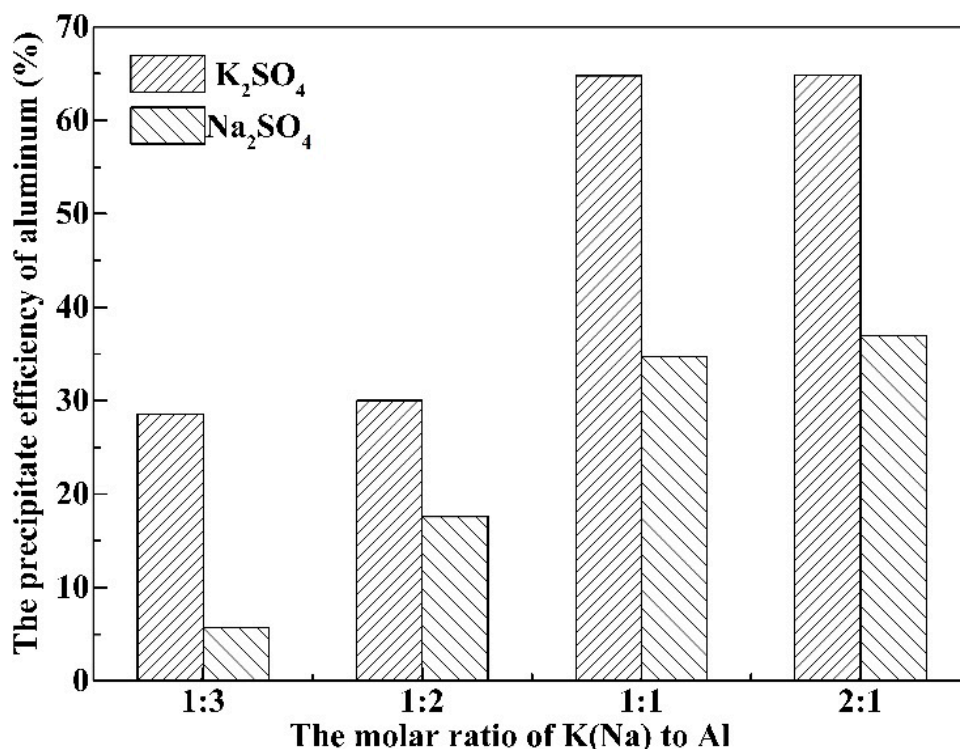


Figure 3. Effect of the K(Na)/Al molar ratio on the precipitation efficiency of aluminum.

As shown in Figure 3, the precipitation efficiency of aluminum increased with increasing amounts of sodium sulfate or potassium sulfate. However, when the K(Na)/Al molar ratio was more than 1:1, increasing the K(Na)/Al molar ratio had no obvious effect on the precipitation efficiency of aluminum, which may be due to the decreasing pH value with the progress of the reaction inhibiting the reaction.

3.3. Effect of Temperature on the Precipitation Efficiency of Al

Experiments were carried out at different temperatures under the following conditions: K(or Na)/Al molar ratio of 1, pH value of 0.4, and reaction time of 5 h. The results are shown in Figure 4.

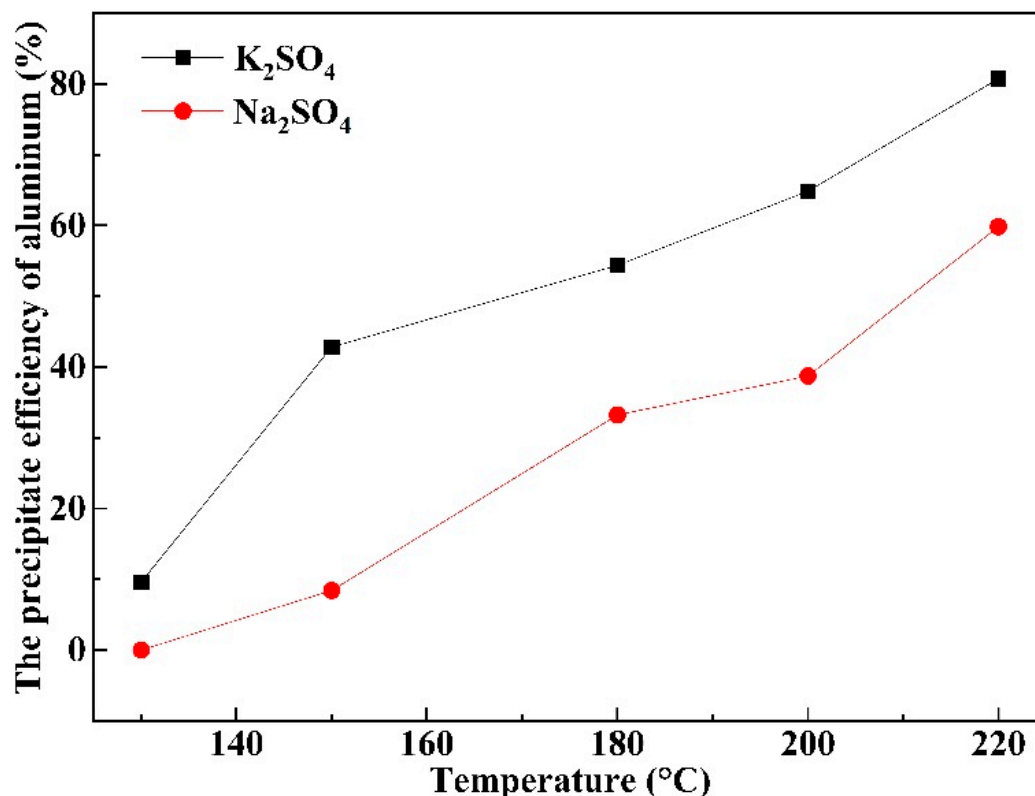


Figure 4. Effect of temperature on the precipitation efficiency of aluminum.

As shown in Figure 4, the temperature significantly influenced the precipitation behavior of aluminum. With increasing temperature, the precipitation efficiency of aluminum increased. However, at the same temperature, the precipitation efficiency of aluminum with the addition of sodium sulfate was lower than that with the addition of potassium sulfate. When the temperature was 220 °C, the precipitation efficiency of aluminum with the addition of potassium sulfate was 81.75%, while the precipitation efficiency of aluminum with the addition of sodium sulfate was 60.83%. The concentration of aluminum decreased from 0.6 mol/L (16.2 g/L) to 2.95 g/L or 6.34 g/L, respectively.

3.4. The Precipitation Thermodynamics and Kinetics of Alunite and Natroalunite

Within the temperature range of 100–350 °C, water can act as a catalytically active species in chemical reactions and possesses a strong tendency to ionize [25,26]. Alunite can be formed by the reaction of K⁺ (Na⁺), Al³⁺, SO₄²⁻ and OH⁻ [20,22,27]. After the reaction, the pH value decreased, and the formation of natroalunite (or alunite) caused by the reaction of Na₂SO₄ (or K₂SO₄) and Al₂(SO₄)₃ can be expressed by Equations (2) and (3). The Gibbs free energy of the reactions was calculated using HSC software. The results are shown in Figure 5.



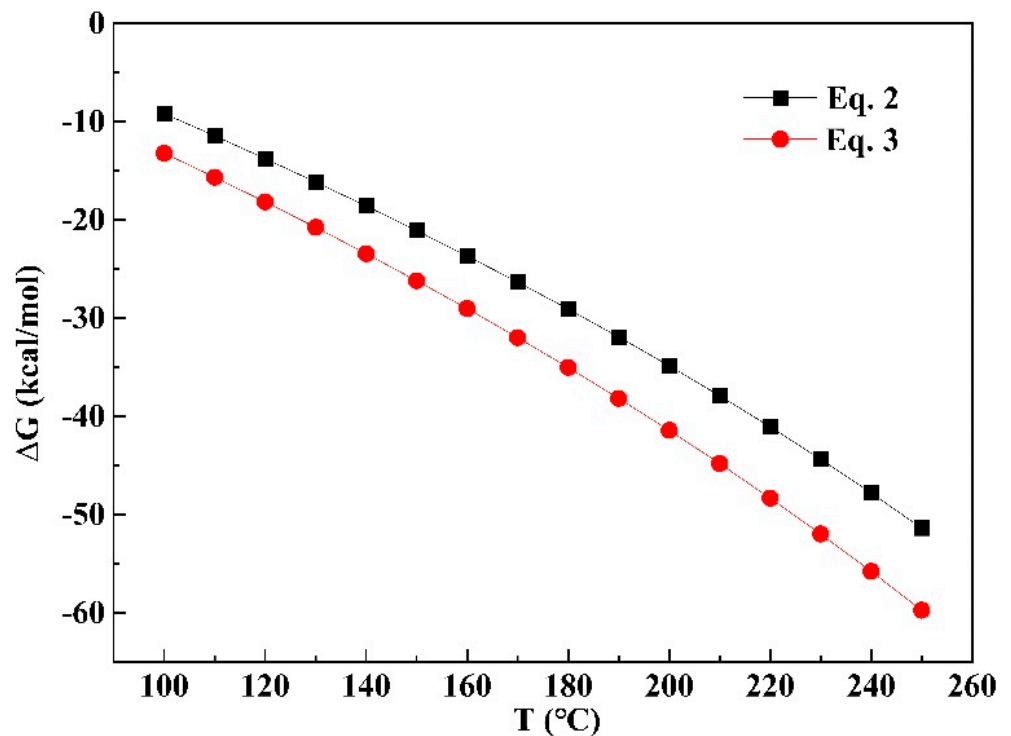


Figure 5. The ΔG^\ominus values of Equations (2) and (3) at different temperatures.

As illustrated in Figure 5, the ΔG^\ominus values were negative at temperatures higher than 100 °C, and decreased with increasing temperature. Equations (2) and (3) were spontaneous when the temperature was higher than 100 °C. In contrast, the ΔG^\ominus values of Equation (3) were lower than those obtained using Equation (2), which indicates that alunite was formed more easily than natroalunite.

The equilibrium compositions of alunite and natroalunite were also analyzed using HSC software under the same thermodynamic conditions. The amount of Al^{3+} , K^+ , Na^+ , SO_4^{2-} and OH^- were set at 1 mol, 1 mol, 1 mol, 1 mol, and 3 mol, respectively. The equilibrium composition diagrams are shown in Figure 6.

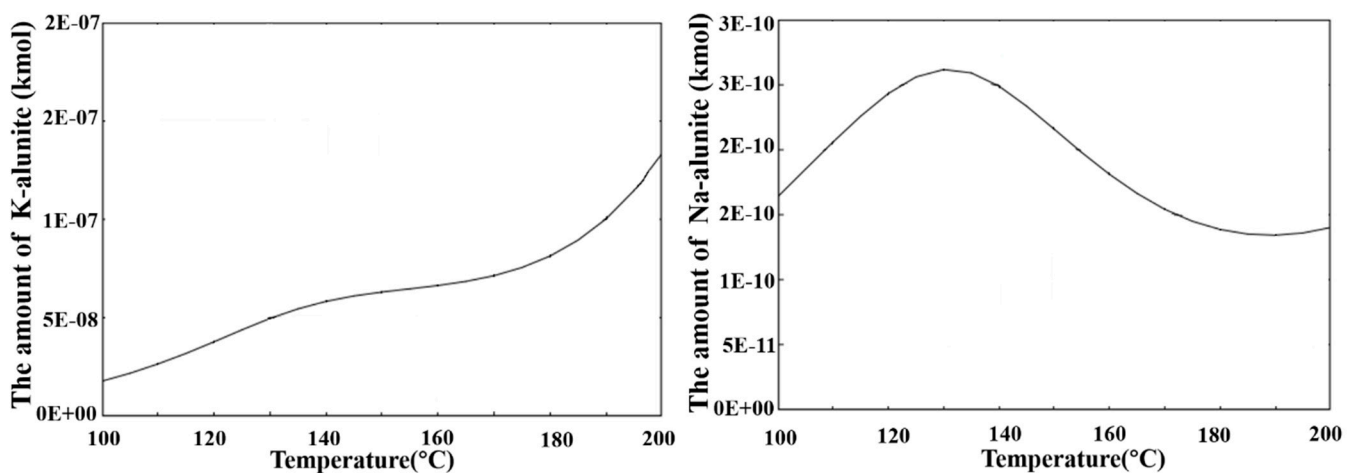


Figure 6. The equilibrium composition diagrams of the $\text{K-Na-SO}_4^{2-}\text{-H}_2\text{O}$ system.

As shown in Figure 6, the amount of alunite is much greater than the amount of natroalunite. However, with increasing temperature, the amount of alunite increased,

while the amount of natroalunite first increased and then decreased. In combination with Figure 5, it can be concluded that increasing temperature promotes the formation of alunite and natroalunite. It is speculated that it is possible to replace Na with K, with the reaction being expressed as in Equation (4), and the relationship between Gibbs free energy and temperature being as shown in Figure 7.

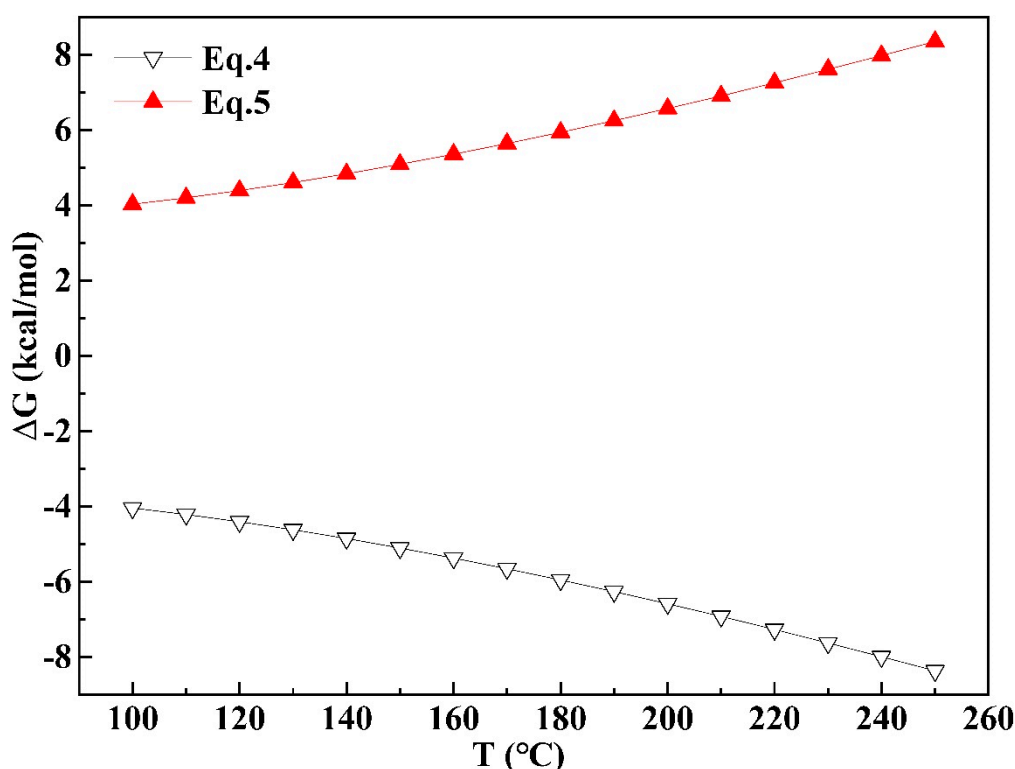
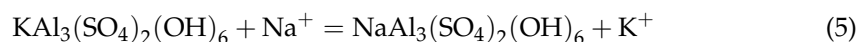


Figure 7. The ΔG^θ values of Equations (4) and (5) at different temperatures.

As shown in Figure 7, the ΔG^θ values are negative for the reaction in Equation (4), but the ΔG^θ values are positive for the reaction in Equation (5). The ΔG^θ values of Equation (4) decrease with increasing temperature, which means that the Na^+ at the A-site of natroalunite can theoretically be replaced with K^+ and transformed into alunite, but the alunite cannot be transformed into natroalunite.

According to the thermodynamic calculation of HSC, under the same conditions, alunite forms more easily than natroalunite. Therefore, the effect of temperature on the kinetics of natroalunite and alunite were preliminarily investigated, and the apparent activation energy was calculated.

The curve of K^+ or Na^+ concentration with reaction time was drawn, as shown in Figure 8. The tangent of the curve was obtained for a specified time, and the rate equation for the reaction can be written as shown in Equation (6).

$$r_i = -\frac{d[C]}{dt_i} \quad (6)$$

where r_i is the reaction rate constant at t_i , t_i is the time of the reaction (min), and $[C]$ is the concentration of K^+ or Na^+ at t_i (g/L).

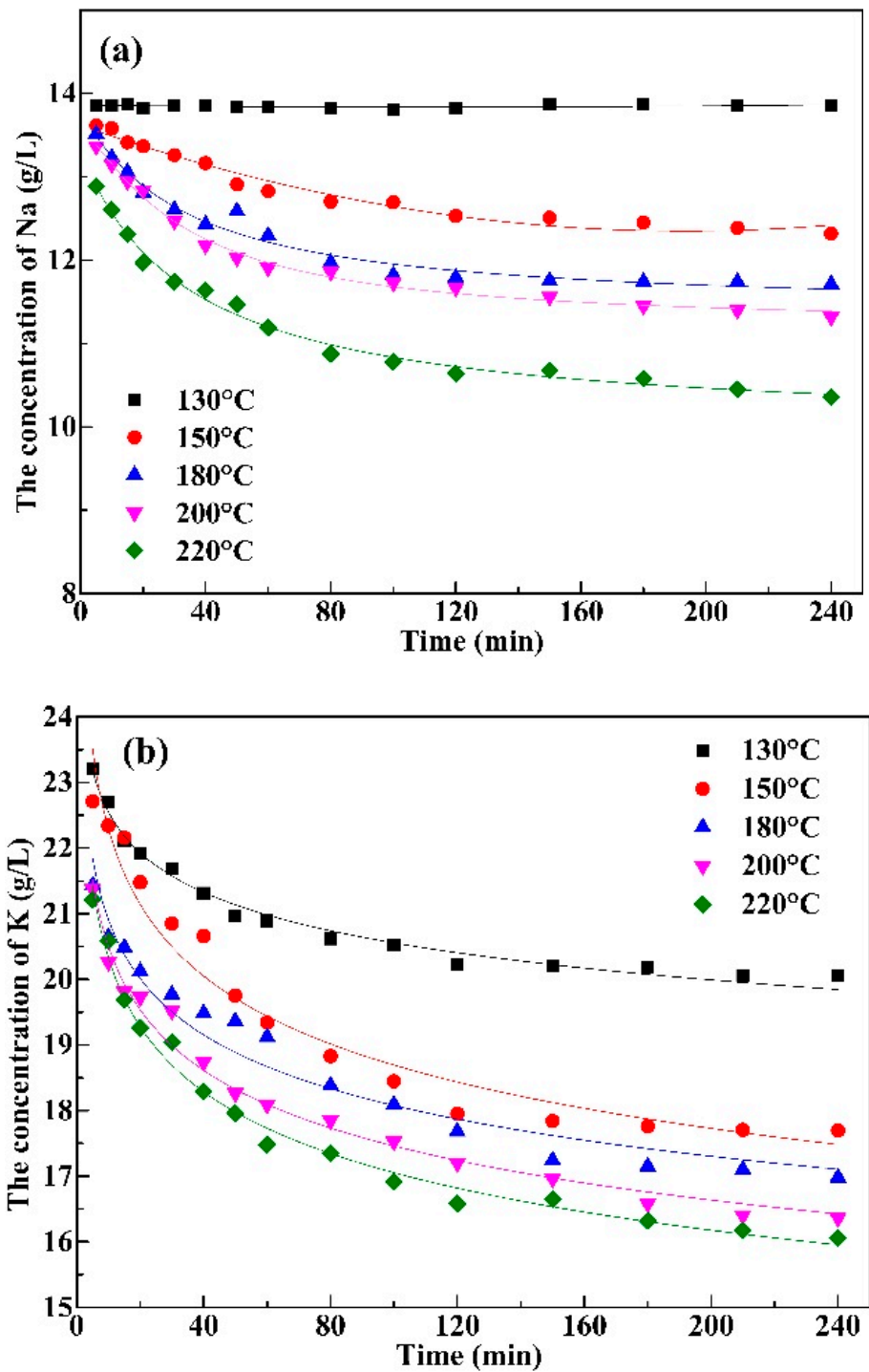


Figure 8. Variation in the concentration of Na⁺ or K⁺ with hydrothermal reaction at different temperatures: (a) Na₂SO₄; (b) K₂SO₄.

The reaction rate and the concentration of K⁺ or Na⁺ conform to the following relationship, see Equation (7), as shown in Figure 9.

$$\ln r_i = \ln k + m \ln [C] \tag{7}$$

where k is the reaction rate constant, and m is the reaction order.

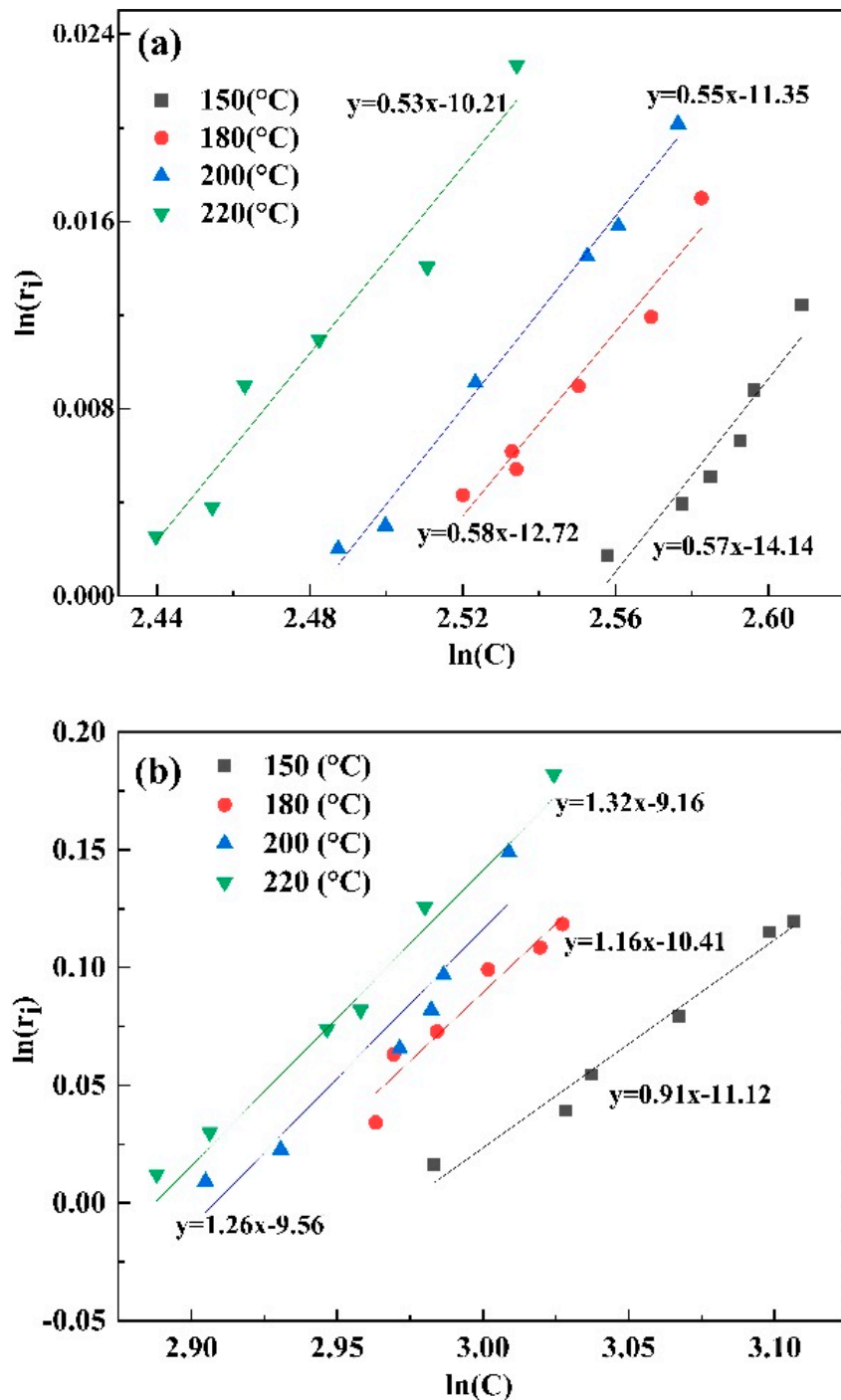


Figure 9. Fitting results of Equation (7) at different temperature: (a) Na_2SO_4 ; (b) K_2SO_4 .

Finally, according to the relationship between the reaction rate constant (k) and temperature (T), the apparent activation energy E_a of natroalunite and alunite were calculated using the Arrhenius formula (see Equation (8)) [28–30], as shown in Figure 10.

$$\ln k = -\frac{E_a}{RT} + A \tag{8}$$

where k is the reaction rate constant, E_a is the apparent activation energy (kJ/mol), R is the molar gas constant ($\text{J}\cdot\text{mol}^{-1}\cdot\text{K}^{-1}$), T is the reaction temperature (K), and A is the constant.

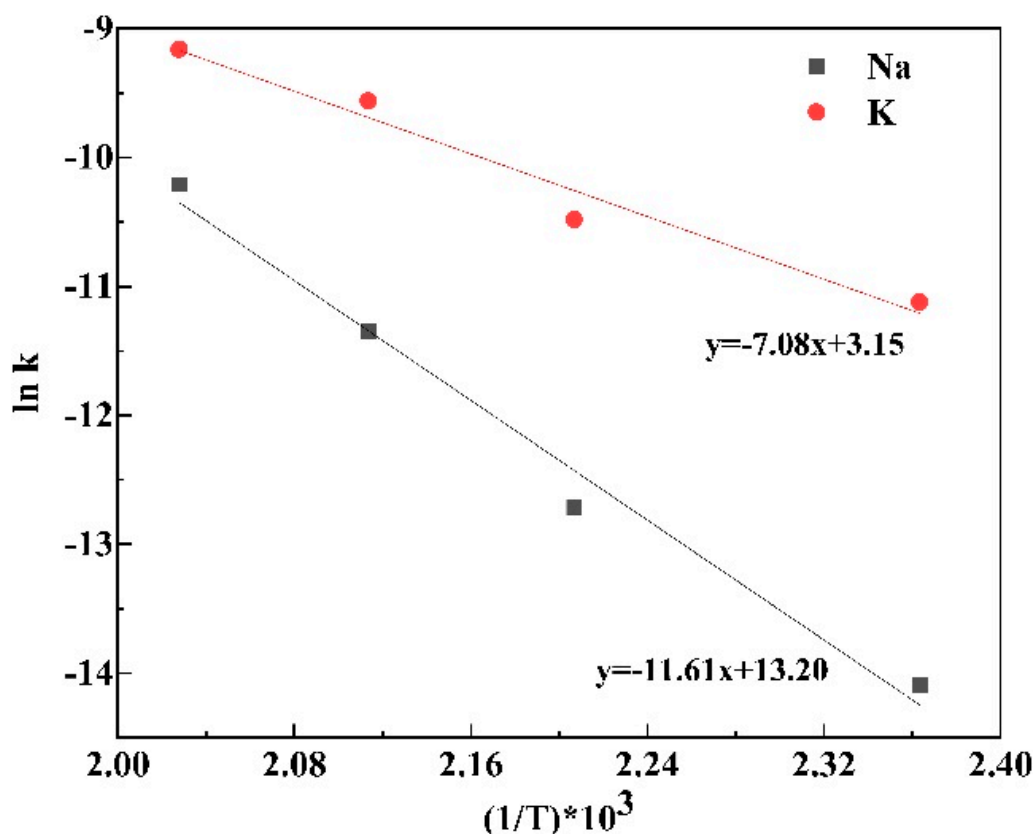


Figure 10. Fitting line of the Arrhenius equation.

It can be concluded from Figure 8 that the reaction rate increased with increasing temperature, and the precipitation efficiency of aluminum increased too. The rate of ion concentration slowed down with increasing reaction time. However, the reaction rate of sodium sulfate and potassium sulfate were different. When the temperature was 130 °C, natroalunite was barely formed, whereas alunite was formed. The precipitation efficiency of natroalunite was lower than that of alunite at the same temperature.

Since the reaction is greatly affected by the temperature, natroalunite was barely formed at a temperature of 130 °C, so only the data obtained at temperatures of 150 °C, 180 °C, 200 °C, and 220 °C were used for the calculation of the apparent activation energy E_a . With increasing reaction time, the instantaneous reaction rate decreased and tended towards flat. Therefore, the apparent activation energy was calculated on the basis of the reaction data for the first hour. As shown in Figure 10, according to the Arrhenius formula, the apparent activation energy of natroalunite was 96.52 kJ/mol, while that of alunite was 58.86 kJ/mol, meaning that alunite was more easily formed than natroalunite, and these reactions were controlled by the chemical reaction.

On the basis of the calculation of the thermodynamic and kinetic properties, it can be seen that both the ΔG^θ values and the activation energy of alunite were lower than those of natroalunite. It can be concluded that alunite is more readily formed than natroalunite under the same conditions.

3.5. Mechanism for the Co-Precipitation of Vanadium and Alunite (Natroalunite)

To analyze the composition of the precipitate, XRD analyses were performed on precipitates obtained at different pH values, as shown in Figure 11.

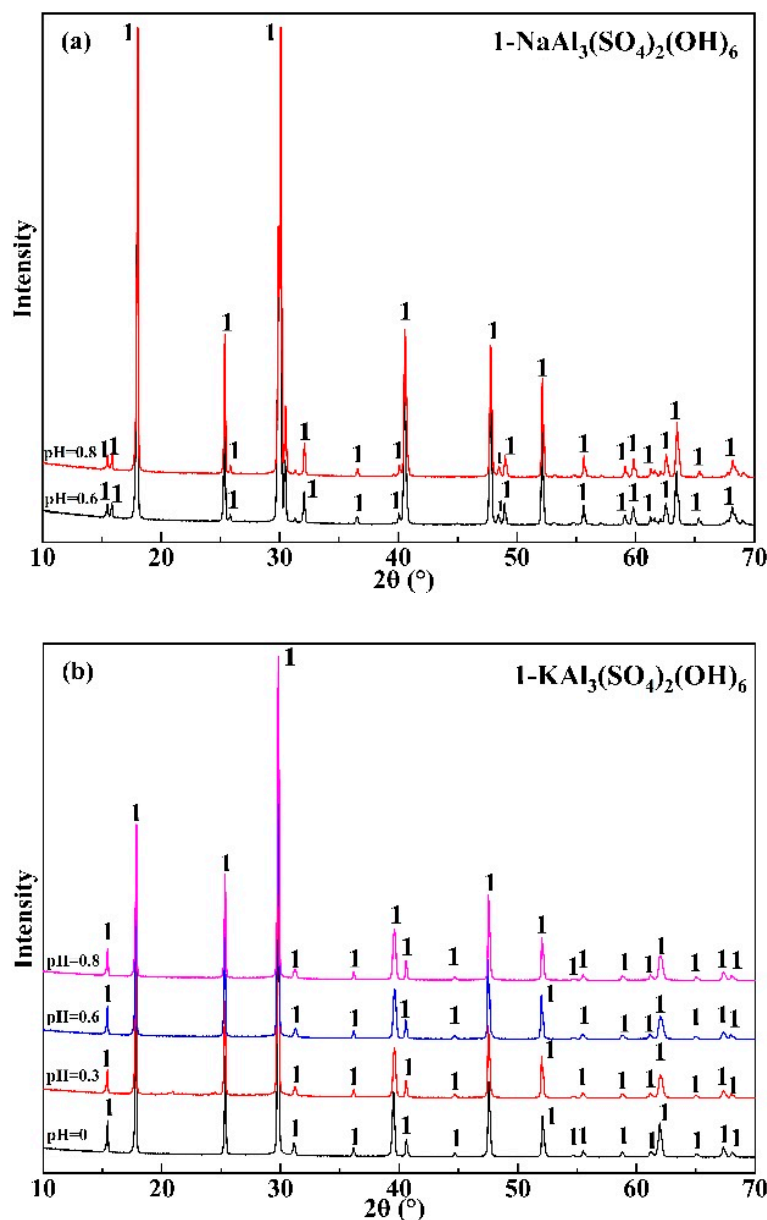


Figure 11. XRD patterns of precipitate obtained by aluminum precipitation experiment: (a) Na₂SO₄; (b) K₂SO₄.

As shown in Figure 11, the intensity of the diffraction peaks in the sample is strong and sharp, and there are no other impurity peaks. Figure 11a (with the addition of sodium sulfate) clearly shows that only natroalunite was formed, and the diffraction peaks at different pH values are almost the same. Figure 11b (with the addition of potassium sulfate) clearly shows that only alunite was formed, and the diffraction peaks at different pH values are almost the same. Thus, in the suitable pH range, alunite and natroalunite can be formed stably. However, the vanadium compounds were not detected, indicating that vanadium may be precipitated in the form of amorphous or adsorbed on the natroalunite or alunite particles during the reaction process.

When the pH value was above 0.4, part of vanadium was co-precipitated during the formation processes of natroalunite and alunite. To directly visualize the behaviors of Al and vanadium during the experimental process, SEM-EDS analyses were conducted, and the results are shown in Figure 12.

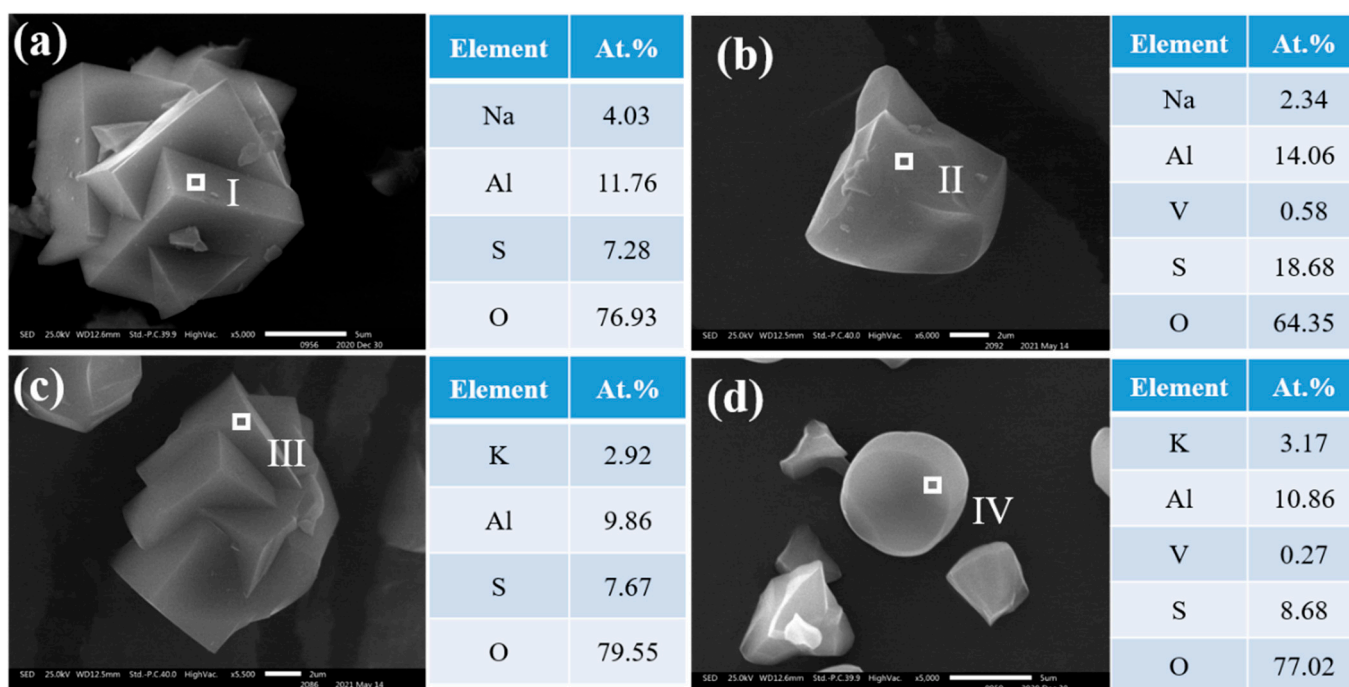


Figure 12. SEM-EDS patterns of samples obtained at pH value of 0.6: (a) Na:Al = 1:1; (b) Na:Al = 1:1; (c) K:Al = 1:1; (d) K:Al = 1:1.

For the detection of SEM-EDS, Na and K have good relevance for the Al, S and O elements, while only a small amount of V was detected in a small number of particles. The particles shown in Figure 12a,b are natroalunite, while the particles shown in Figure 12c,d are alunite. In Figure 12a,c, the particles possess a good crystal form without the detection of vanadium. However, in Figure 12b,d, the crystal morphology is not as complete as that shown in Figure 12a,c, and a small amount of vanadium was detected. Thus, vanadium may be adsorbed due to incomplete crystal growth.

To further analyze the precipitation behavior of vanadium, the samples were analyzed by XPS. The XPS analysis was carried out as illustrated in Figure 13.

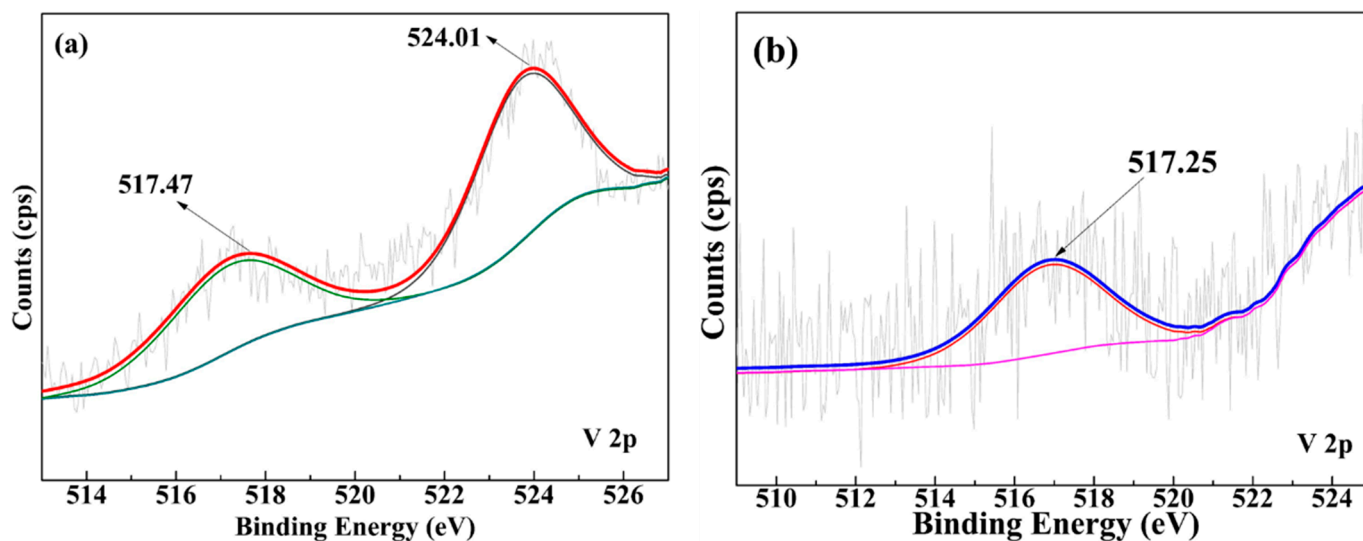


Figure 13. The XPS analysis of samples obtained at pH value of 0.6: (a) Na₂SO₄; (b) K₂SO₄.

As shown in Figure 13, a V 2 p peak with a binding energy of 517.47 eV and 524.01 eV was detected in natroalunite, while a V 2 p peak with a binding energy of 517.25 eV was detected in alunite. The V 2 p peaks with binding energies of 517.47 eV, 517.28 eV and 524.01 eV belong to the V(V)-O bond [31–33]. In the acid leachate of black shale, vanadium mainly exists in a tetravalent form, and the valence state of the vanadium used in the experiment was tetravalent too. This indicates a change in the chemical environment of V during the precipitation process of alunite. A few V(IV) ions were oxidized to V(V) ions, which were precipitated with aluminum.

Under hydrothermal conditions, the dissolution efficiency of oxygen is increased [26], vanadium can be oxidized by oxygen, and transformed into a pentavalent form. According to the potential–pH diagram for vanadium–water systems at 298 K [34], the form of vanadium present is different at different concentrations and valence states of vanadium, V(IV) exists in the form of VO^{2+} , and V(V) exists in the form of VO_2^+ or $\text{HV}_{10}\text{O}_{28}^{5-}$ at low pH values. The V(IV) oxidation reaction can be expressed by Equations (9) and (10), and the ΔG^θ values are shown in Figure 14.

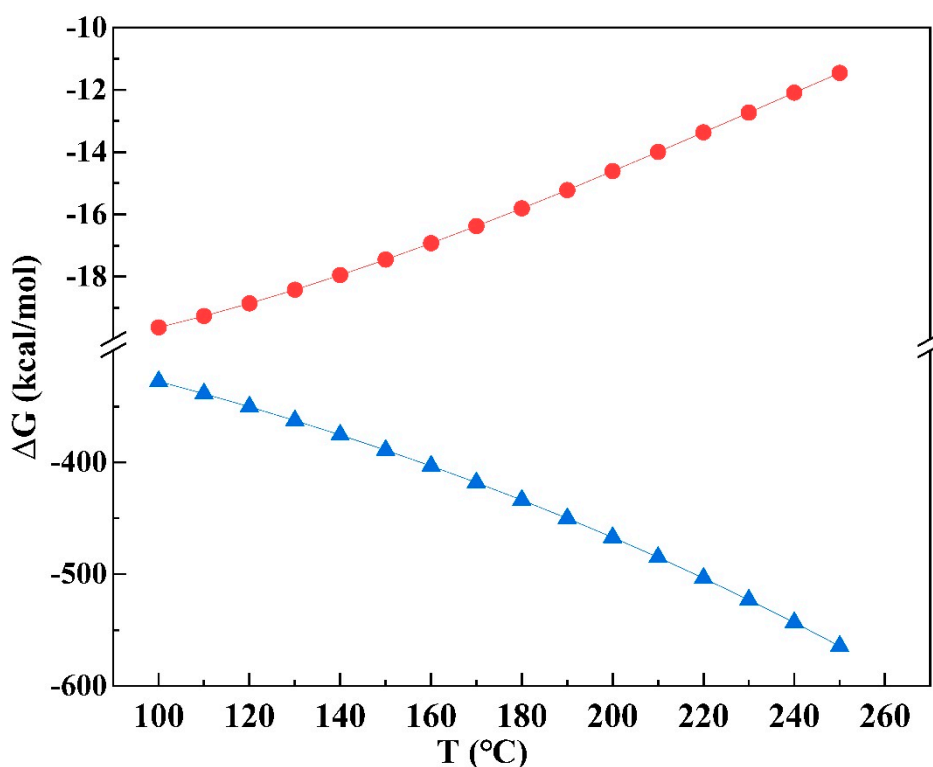
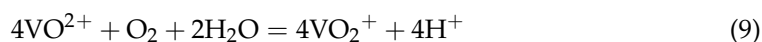


Figure 14. The ΔG^θ values of Equations (9) and (10) at different temperatures.

As shown in Figure 13, the ΔG^θ values were negative for Equations (9) and (10), with ΔG^θ values decreasing with an increase in temperature. Therefore, the oxidation of V(IV) by oxygen can occur spontaneously under hydrothermal conditions.

Zeta potential analysis of alunite with and without vanadium was carried out, and the results are shown in Figure 15.

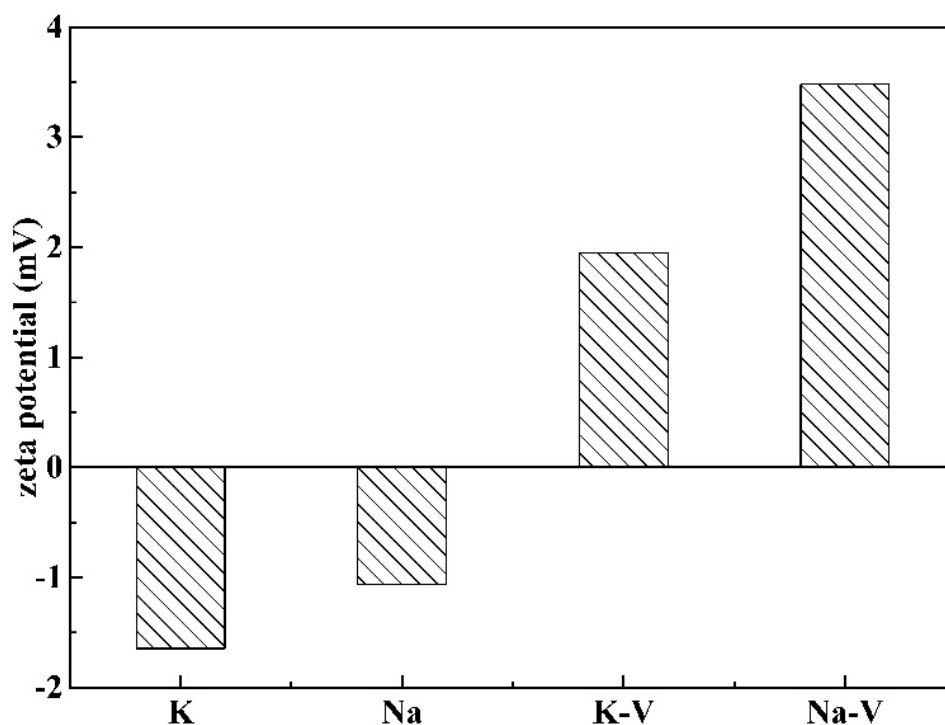


Figure 15. The zeta potentials of the precipitates at a pH value of 0.6 ((K) alunite; (Na) natroalunite; (K-V) alunite with co-precipitated vanadium; (Na-V) natroalunite with co-precipitated vanadium).

As shown in Figure 15, the zeta potentials of alunite and natroalunite without co-precipitated vanadium are negative. In the lattice structures of natroalunite and alunite, the octahedral structure of $\text{AlO}_2(\text{OH})_4$ is connected with the tetrahedral structure of SO_4^{2-} , and the Na(K) ions are coordinated with the O atoms and OH groups as $\text{AO}_6(\text{OH})_6$, located in an icosahedra site. In addition, the hydroxyl anion, OH^- , is located at the junction of octahedral and icosahedra [34]. The hydrogen bonds between the apical oxygen of the S-O bond and the hydroxyl group from the octahedra cause deformations of the tetrahedra and octahedra [16]. According to zeta potential analysis, the zeta potentials of alunite and natroalunite with co-precipitated vanadium were increased and positive. It can be concluded that the V(V) is present, and was adsorbed in the form of cation VO_2^+ , with vanadium loss being caused by electrostatic adsorption.

4. Conclusions

It is feasible to separate aluminum over vanadium through the formation of alunite and natroalunite. In hydrothermal environments, alunite and natroalunite are able to stably form during the process of Al^{3+} hydrolysis precipitation at a temperature of 220 °C, a pH value of 0.4, and a reaction time of 5 h. When Al^{3+} was precipitated at a K/Al molar ratio of 1, the precipitation efficiency of aluminum was 81.75% via the formation of alunite, and the concentration of aluminum decreased from 16.2 g/L to 2.95 g/L. When Al^{3+} was precipitated with an Na/Al molar ratio of 1, the precipitation efficiency of aluminum was 60.83% via the formation of natroalunite, and the concentration of aluminum decreased from 16.2 g/L to 6.34 g/L. The ΔG^θ values of the formation of alunite and natroalunite are negative at temperatures higher than 100 °C and decrease with increasing temperature. At the same temperature, the ΔG^θ value of alunite is lower than that of natroalunite; therefore, alunite forms more easily than natroalunite. The apparent activation energy of natroalunite is 96.52 kJ/mol, whereas the apparent activation energy of alunite is 58.86 kJ/mol. The reaction rate increases with increasing temperature, and precipitation is controlled by the chemical reaction. The zeta potentials of the alunite and natroalunite surfaces are negative, whereas the zeta potentials of alunite and natroalunite

with co-precipitated vanadium are increased and are positive. Vanadium loss increases with increasing pH value. It can be deduced that the ion state of tetravalent vanadium (VO^{2+}) transformed into a pentavalent vanadium (VO_2^+) ion state in the hydrothermal environment. The VO_2^+ can be adsorbed onto the alunite or natroalunite due to their negative surface charges, ultimately leading to vanadium loss. To avoid vanadium loss, the pH value should not be over 0.4.

Author Contributions: Conceptualization, L.W. and N.X.; methodology, Y.Z., P.H.; software, L.W.; validation, N.X.; formal analysis, L.W. and N.X.; resources, Y.Z.; data curation, L.W.; writing—original draft preparation, L.W.; writing—review and editing, L.W. and N.X.; visualization, Y.Z.; project administration, Y.Z.; funding acquisition, N.X. and P.H. All authors have read and agreed to the published version of the manuscript.

Funding: This research was funded by the Project of National Natural Science Foundation of China (No. 51804226& 52004187) and the Outstanding Young and Middle-aged Science and Technology Innovation Team Project of Hubei Province (T201802).

Data Availability Statement: Data are available on request to the authors.

Conflicts of Interest: The authors declare no conflict of interest.

References

- Chen, X.X.; Wang, H.; Yan, B.J. Sulfuric acid leaching and recovery of vanadium from a spinel concentrate beneficiated from stone coal ore. *Hydrometallurgy* **2020**, *191*, 105239. [[CrossRef](#)]
- Huang, Z.L.; Chen, T.; Zhou, Y.; Xu, W.B.; Lin, H.Z.; Yan, B. Optimization of oxidative leaching for vanadium extraction from low-grade stone coal using response surface methodology. *Process* **2020**, *8*, 1534. [[CrossRef](#)]
- Zhang, C.Q.; Sun, C.Y.; Li, H.; Yin, W.Z.; Zhou, J.J. Blank roasting kinetics of illite type vanadium bearing stone coal. *J. Mater. Res. Technol.* **2020**, *9*, 7363–7369. [[CrossRef](#)]
- Zhang, Y.B.; Zhang, Q.; Cai, Y.; Wang, D.P.; Li, K.W. The occurrence state of vanadium in the black shale-hosted vanadium deposits in Shangling of Guangxi Province, China. *Chin. J. Geochem.* **2015**, *34*, 484–497. [[CrossRef](#)]
- Zheng, Q.S.; Zhang, Y.M.; Xue, N.N.; Liu, T.; Huang, J. Vanadium occupation and its leachability differences in trioctahedral and dioctahedral mica. *RSC Adv.* **2019**, *9*, 27615–27624. [[CrossRef](#)]
- Wang, F.; Zhang, Y.M.; Liu, T.; Huang, J.; Zhao, J.; Zhang, G.B.; Liu, J. A mechanism of calcium fluoride-enhanced vanadium leaching from stone coal. *Int. J. Miner. Process* **2016**, *145*, 87–93. [[CrossRef](#)]
- Zhu, X.B.; Zhang, Y.M.; Huang, J.; Liu, T.; Wang, Y. A kinetics study of multi-stage counter-current circulation acid leaching of vanadium from stone coal. *Int. J. Miner. Process* **2012**, *114–117*, 1–6. [[CrossRef](#)]
- Zhang, Y.M.; Zhu, X.B.; Liu, T.; Huang, J.; Song, S.X. Effect of colloidal potassium alum formation on vanadium recovery from acid leach solutions of stone coal. *Hydrometallurgy* **2013**, *138*, 54–58. [[CrossRef](#)]
- Li, W.; Zhang, Y.M.; Liu, T.; Huang, J.; Wang, Y. Comparison of ion exchange and solvent extraction in recovering vanadium from sulfuric acid leach solutions of stone coal. *Hydrometallurgy* **2013**, *131–132*, 1–7. [[CrossRef](#)]
- Shi, Q.H.; Zhang, Y.M.; Huang, J.; Liu, T.; Liu, H.; Wang, L.Y. Synergistic solvent extraction of vanadium from leaching solution of stone coal using D2EHPA and PC88A. *Sep. Purif. Technol.* **2017**, *181*, 1–7. [[CrossRef](#)]
- Shi, Q.H.; Zhang, Y.M.; Liu, T.; Huang, J.; Liu, H. Two-stage separation of V(IV) and Al(III) by crystallization and solvent extraction from aluminum-rich sulfuric acid leaching solution of stone coal. *JOM* **2017**, *69*, 1950–1957. [[CrossRef](#)]
- Wang, Y.D.; Li, J.H.; Gao, Y.; Yang, Y.; Gao, Y.; Xu, Z.F. Removal of aluminum from rare-earth leaching solutions via a complexation-precipitation process. *Hydrometallurgy* **2020**, *191*, 105220. [[CrossRef](#)]
- Wang, X.W.; Wang, H.G.; Gao, D.X.; Chen, B.F.; Meng, Y.Q.; Wang, M.Y. A clean technology to separate and recover vanadium and chromium from chromate solutions. *Hydrometallurgy* **2018**, *177*, 94–99. [[CrossRef](#)]
- Wang, M.Y.; Chen, B.F.; Huang, S.; Wang, X.W.; Liu, B.; Ge, Q.; Xie, S.S. A novel technology for vanadium and chromium recovery from V-Cr-bearing reducing slag. *Hydrometallurgy* **2017**, *171*, 116–122. [[CrossRef](#)]
- Guo, Y.X.; Lv, H.B.; Yang, X.; Cheng, F.Q. $\text{AlCl}_3\text{-6H}_2\text{O}$ recovery from the acid leaching liquor of coal gangue by using concentrated hydrochloric impouring. *Sep. Purif. Technol.* **2015**, *151*, 177–183. [[CrossRef](#)]
- Frost, R.L.; Wills, R.; Weier, M.L.; Martens, W.; Theo Klopogge, J. A Raman spectroscopic study of alunites. *J. Mol. Struct.* **2006**, *785*, 123–132. [[CrossRef](#)]
- Maubec, N.; Lahfid, A.; Lerouge, C.; Wille, G.; Michel, K. Characterization of alunite supergroup minerals by Raman spectroscopy. *Spectrochim. Acta Part A Mol. Biomol. Spectrosc.* **2012**, *96*, 925–939. [[CrossRef](#)] [[PubMed](#)]
- Dutrizac, J.E.; Jambor, J.L. Jarosites and their application in hydrometallurgy. *Rev. Mineral. Geochem.* **2000**, *40*, 405–452. [[CrossRef](#)]
- Rudolph, W.W.; Mason, R.; Schmidt, P. Synthetic alunites of the potassium-oxonium solid solution series and some other members of the group: Synthesis, thermal and X-ray characterization. *Eur. J. Miner.* **2003**, *15*, 913–924. [[CrossRef](#)]

20. Viñals, J.; Sunyer, A.; Molera, P.; Cruells, M.; Llorca, N. Arsenic stabilization of calcium arsenate waste by hydrothermal precipitation of arsenical natroalunite. *Hydrometallurgy* **2010**, *104*, 247–259. [[CrossRef](#)]
21. Xu, H.; Zhu, B.; Ren, X.; Shao, D.; Tan, X.; Chen, C. Controlled synthesized natroalunite microtubes applied for cadmium(II) and phosphate co-removal. *J. Hazrad. Mater.* **2016**, *314*, 249–259. [[CrossRef](#)]
22. Zhu, B.S.; Jia, Y.; Jin, Z.; Sun, B.; Luo, T.; Yu, X.Y.; Kong, L.T.; Huang, X.J.; Liu, J.H. Controlled synthesis of natroalunite microtubes and spheres with excellent fluoride removal performance. *Chem. Eng. J.* **2015**, *271*, 240–251. [[CrossRef](#)]
23. Xue, N.; Zhang, Y.M.; Huang, J.; Liu, T.; Wang, L.Y. Separation of impurities aluminum and iron during pressure acid leaching of vanadium from stone coal. *J. Clean Prod.* **2017**, *166*, 1265–1273. [[CrossRef](#)]
24. Huang, J.; Zhang, Y.M.; Huang, J.; Liu, T.; Cai, Z.L.; Xue, N.N. Selective leaching of vanadium from roasted stone coal by dilute sulfuric acid dephosphorization-two-stage pressure acid leaching. *Minerals* **2016**, *6*, 75. [[CrossRef](#)]
25. Tester, J.W.; Cline, J.A. Hydrolysis and oxidation in subcritical and supercritical water: Connecting process engineering science to molecular interactions. *Cor. Eng. Sect.* **1999**, *55*, 1088–1100. [[CrossRef](#)]
26. Marshall, W.L.; Franck, E.U. Ion product of water substance, 0–1000 °C, 1–10,000 bars new international formulation and its background. *J. Phys. Chem. Ref. Data* **1981**, *10*, 295–304. [[CrossRef](#)]
27. Sunyer, A.; Viñals, J. Arsenate substitution in natroalunite: A potential medium for arsenic immobilization. Part 2: Cell parameters and stability tests. *Hydrometallurgy* **2011**, *109*, 106–115. [[CrossRef](#)]
28. Croker, D.; Loan, M.; Hodnett, B.K. Kinetics and mechanisms of the hydrothermal crystallization of calcium titanate species. *Cryst. Growth Des.* **2009**, *9*, 2207–2213. [[CrossRef](#)]
29. Du, G.C.; Sun, Z.H.; Xian, Y.; Jing, H.; Chen, H.J.; Yin, D.F. The nucleation kinetics of ammonium metavanadate precipitated by ammonium chloride. *J. Cryst. Growth* **2016**, *441*, 117–123. [[CrossRef](#)]
30. Le, T.K.; Kang, M.; Tran, V.T.; Kim, S.W. Relation of photoluminescence and sunlight photocatalytic activities of pure V2O5 nanohollows and V2O5/RGO nanocomposites. *Mat. Sci. Semicon. Proc.* **2019**, *100*, 159–166. [[CrossRef](#)]
31. Vaschetti, V.M.; Eimer, G.A.; Cánepa, A.L.; Casuscelli, S.G. Catalytic performance of V-MCM-41 nanocomposites in liquid phase limonene oxidation: Vanadium leaching mitigation. *Micropor. Icropor. Mesopor. Mat.* **2021**, *311*, 110678. [[CrossRef](#)]
32. NIST XPS Database. Available online: <https://srdata.nist.gov/xps/intro.aspx> (accessed on 15 May 2021).
33. Zhou, X.J.; Wei, C.; Li, M.T.; Qiu, S.; Li, X.B. Thermodynamics of vanadium–Sulfur–Water systems at 298K. *Hydrometallurgy* **2011**, *106*, 104–112. [[CrossRef](#)]
34. Sato, E.; Nakai, I.; Miyawaki, R.; Matsubara, S. Crystal structures of alunite family minerals: Beaverite, corkite, alunite, natroalunite, jarosite, svanbergite, and woodhouseite. *Neues Jahrb. Mineral. Abh.* **2009**, *185*, 313–322. [[CrossRef](#)]